Electron density analysis of metal clusters with semi-interstitial main group atoms. Chemical bonding in $[Co_6X(CO)_{16}]^-$ species.

S. Racioppi[†§*], *R. Della Pergola*[‡], *V. Colombo*[†], *A. Sironi*[†], *P. Macchi*[§*]

†Università degli Studi di Milano, Dipartimento di Chimica a– Via Golgi, 19 – 20133 Milano Italy

‡Università di Milano-Bicocca- Dipartimento di Scienze Ambientali e della Terra, piazza della Scienza 1 – 20126 Milano Italy

[§]University of Bern - Department of Chemistry and Biochemistry, Freiestrasse 3 - 3012 Bern – Switzerland

ABSTRACT

In this work, we propose a careful and thorough analysis of the chemical bond nature in high nuclearity metal carbonyl clusters having semi-interstitial main group atoms. We investigated the species $[Co_6X(CO)_{16}]^-$ (X= As, P), known for a rather interesting conformational flexibility of the cluster (leading to open or closed cages) and a corresponding polymorphism in solid state (observed at least for X = As). The factors that trigger the molecular isomerism and the nature of X-Co and Co-Co interactions emerge from theoretical calculations and high resolution X-ray diffraction. Both energy and charge density atomic partitioning (QTAIM, EDA, IQA) are employed for this analysis, with the aim of revealing the

stabilizing/destabilizing factors of the interaction between the cage and the semi-interstitial atoms in the various conformations.

1. INTRODUCTION

Since the discovery of the first high nuclearity ($n \geq 6$) metal carbonyl cluster, $[Co_6(CO)_{15}]^{2-}$ in 1967 by Chini,[1] many investigations on these intriguing species have been carried out in order to understand and rationalize the chemical bonding, to predict molecular structures and to investigate their potential catalytic activity. Even before the characterization of $[Co_6(CO)_{15}]^{2-}$, the nuclearity of a cluster could be increased using p-block atoms, following the discovery of $[Fe_5C(CO)_{15}]$.[2] Afterwards, Vidal synthesized and characterized the first high nuclearity clusters featuring interstitial elements of group V, namely $[Rh_9P(CO)_{21}]^{2-}$,[3] $[Rh_{10}P(CO)_{22}]^{3-}$,[4] and $[Rh_{10}As(CO)_{22}]^{3-}$.[5] Finally, using the relatively large atomic radius of pnictogens, combined with their ability to stabilize unusual geometry, Chini *et al.*[6] isolated semi-interstitial anionic clusters, like $[Co_6(CO)_{16}P]^-$. The organometallic chemistry community recently rehashed the interest on these compounds, when other high nuclearity clusters have been reported.[7,8,9] Some carbonyl clusters with semi-interstitial, exposed group V atoms have shown high catalytic performance in the C-H activation of 3-picoline.[10] Moreover, cobalt-phosphide materials are extremely efficient in both hydrogen and oxygen evolution reactions (HER, OER),[11,12] whereas some metal-As carbonyls were found to be promising for magnetic properties.[13]

Transition-metal clusters have always attracted the curiosity of theoretical chemists because of the elusive nature of the metal-metal bonds and the cooperative σ-donation/π-back-donation mechanism of the metal-ligand interactions. The research studies published in the last twenty years made use of different theoretical approaches in order to rationalize the nature of chemical bonding, including charge density analysis[14] or energy decomposition analysis.[15] From some of these studies, it emerged, for example, that

the radial W-Au bonds, the aurophilic interactions and relativistic effects stabilize the icosahedral WAu_{12} cluster,[16] a molecule that was theoretically predicted by Pyykkö before its observation in the gas-phase. Hopffgarten and Frenking[17] studied a number of icosahedral $[M(EH)_{12}]$ compounds, using theoretical tools for an accurate analysis of the nature of the M-E and E-E interactions and for quantifying the atomic contributions to the stability of the molecular structure.

The nature of bonding between metals and interstitial or semi-interstitial main group atoms is still largely unexplored, especially from the point of view of charge density analysis. This prompted us to investigate theoretically and experimentally a class of semi-interstitial carbonyl clusters, namely $[Co_6X(CO)_{16}]^-$ (X = As, P; hereinafter **1** and **2** respectively). As we recently reported,[9] this cluster has two conformers,[i] differing for the presence or absence of a short Co-Co distance (namely Co1-Co2). Hereinafter, the isomers are named **a** and **b**, respectively. For X = As, both isomers (**1a** and **1b**) have been isolated and structurally characterized[9] as salts of tetraphenylphosphonium. For X = P only isomer **2a**, with short Co-Co distance, has been isolated, so far.[6] The species **2b**, *i.e.*, $[Co_6P(CO)_{16}]^-$ with long Co1-Co2 distance, has not been observed yet, at least in the form of a single crystal. In fact, from X-ray diffraction studies, α-**1**$[PPh_4]$ and α-**2**$[PPh_4]$, containing **1a** and **2a** cluster units respectively, crystallize in the P $2_1/c$ space group and are isomorphous whereas β-**1**$[PPh_4]$, having **1b** unit, is a polymorph which crystallizes in the P bca space group. This intriguing stereochemical flexibility and the promising applications of this class of compounds (catalysis, HER/OER, magnetic nanomaterials, etc.), motivated us to carry out an in-depth investigation on the nature of X-Co and Co-Co interaction, using both charge density and energy partition approaches:

[i] Because in both cases a clear Co-Co bond cannot be identified (as discussed in the rest of this paper), we prefer using here the term "conformational isomers", which are in fact due to different rotation of some $Co(CO)_3$ groups, leading to a short or a long Co1-Co2 distance.

Quantum Theory of Atoms in Molecules (QTAIM)[18], Energy decomposition Analysis (EDA)[19], Interacting Quantum Atoms (IQA)[20] and Wiberg Bond Indices (WBI)[21]. For species **2a**, a high resolution X-ray diffraction experiment was also possible, that enabled an experimental model[22] of the charge density distribution, in order to complement and validate the theoretical analysis.

2. THEORY

2.1 Electron Density and its partitioning

The Quantum Theory of Atoms in Molecules, developed by Bader[18], has been extensively adopted both by theoreticians and experimentalists because it is based on a quantum mechanical observable, namely the electron density $\rho(\mathbf{r})$, that can be obtained *via* quantum chemical calculations as well as x-ray diffraction experiments[23]. Through a topological analysis of the total electron density, it is possible to determine atomic volumes (called basins) and analyze the critical points (where $\nabla\rho(\mathbf{r}) = 0$) on the base of the rank and signature of the Hessian matrix: (rank = 3, signature = -3) are local maxima corresponding to nuclear positions; (3,-1) are saddle points, also called *bond critical point*s because found along the line of connection between two atoms (*bond path*), although they do not necessarily correspond to a two-center chemical bond; (3,+1) are ring critical points and (3,+3) are local minima (cage critical points), occurring within cages. QTAIM offers a unique and exact partition of the space and atomic properties (*e.g.* atomic charges, but also atomic energies) can be calculated from the integration over atomic basins. Moreover, the analysis of the Laplacian of the electron density $\nabla^2\rho(\mathbf{r})$, or better $L(\mathbf{r}) = -\nabla^2\rho(\mathbf{r})$, provides a useful representation of the electronic distribution around an atom, defining regions of charge concentrations ($\nabla^2\rho(\mathbf{r}) < 0 \equiv L(\mathbf{r}) > 0$) and charge depletion ($\nabla^2\rho(\mathbf{r}) > 0 \equiv L(r) < 0$). In particular, the formers can be associated with the localization of electron-pairs, providing a physical connection with the VSEPR theory[24].

2.1.1 Refinement of electron density from X-ray diffraction

In order to refine a model from X-ray scattering intensities, the electron density is considered as the sum of atomic electron densities (called pseudo-atoms):

$$\rho_{unit\ cell}(\mathbf{r}) = \sum_i \rho_i(\mathbf{r} - \mathbf{r}_i) \quad (1)$$

$\mathbf{r}_i$ is the position of the atomic nucleus i. In the Hansen & Coppens formalism,[22] each pseudo-atom is further expanded as follow:

$$\rho_i(\mathbf{r}) = P_{i,core}\rho_{i,core}(\mathrm{r}) + P_{i,valence}\kappa_i^3\rho_{i,valence}(\kappa_i\mathbf{r}) + \sum_{l=0,l_{max}}\sum_{m=0,l} P_{i,lm\pm}y_{lm\pm}(\mathbf{r}/\mathrm{r})\kappa'^3_{i,lm\pm}R_{i,lm\pm}(\kappa'_{i,lm\pm}\mathbf{r}) \quad (2)$$

P_i are population parameters, κ are contraction/expansion parameters, $\rho(\mathbf{r})$ are spherically averaged Hartree-Fock or Dirac-Fock density functions of the free atom for core and valence. The last term in the equation is a summation of deformation functions described by a radial term $R(\mathbf{r})$, a normalized single Slater-type density function, multiplied by density-normalized spherical harmonics $y(\mathbf{r}/\mathrm{r})$ up to a given order (in our models $l_{max} = 4$). The multipolar expansion can be formulated also in reciprocal space for the atomic contribution to the unit cell structure factors $|F(\mathbf{h})|$ (where $\mathbf{h}$ is the scattering vector). If experimentally measured x-ray diffraction intensities are available, they can be used to refine the population coefficients of the pseudoatoms using a least-square minimization of the differences between observed and computed structure factors. From the multipolar expansion, all atomic or molecular electrostatic moments and topological indices become easily available.[25]

2.2 Breakdown of Interaction energy

2.2.1 Interacting Quantum Atoms

The Interacting Quantum Atoms (IQA) approach was proposed by Blanco *et al.*[20]. It adopts the real space partition of QTAIM for the whole first order density matrix, in order to obtain intra- and inter- atomic energy contributions:

$$E = \sum_A (T^A + V_{en}^{AA} + V_{ee}^{AA}) + \frac{1}{2}\sum_{A\neq B}(V_{nn}^{AB} + V_{en}^{AB} + V_{ne}^{AB} + V_{ee}^{AB}) = \sum_A E_{self}^A + \frac{1}{2}\sum_{A\neq B} E_{int}^{AB} \quad (3)$$

where A ≡ Ω_A is the atomic basin of nucleus A; T^A is its atomic kinetic energy; and V_{en}, V_{ne}, V_{ee}, and V_{nn} are the potential energies describing the pairwise interactions between the electrons and nuclei of basin A and B. The sum of all the intra-basin terms (A) defines the *self-energy* of a quantum atom (E_{self}^A) or a group of atoms $\mathcal{H}$ ($E_{self}^{\mathcal{H}}$), whereas the inter-basin ones correspond to the interaction energy between atom pairs, E_{int}^{AB}. A further partition of E_{int}^{AB} is possible into a classical term V_{cl}^{AB} and an exchange-correlation term V_{xc}^{AB}:

$$E_{int}^{AB} = V_{cl}^{AB} + V_{xc}^{AB} \quad (4a)$$

$$V_{xc}^{AB} = V_{ee}^{AB} - V_C^{AB} \quad (4b)$$

$$V_{cl}^{AB} = V_{nn}^{AB} + V_{en}^{AB} + V_{ne}^{AB} + V_C^{AB} \quad (4c)$$

where V_C^{AB} is the Coulombic part of V_{ee}. V_{cl}^{AB} and V_{xc}^{AB} can be associated with the classical notions of ionicity and covalency respectively.[26]

As suggested by Cukrowski[27], the contribution of a molecular fragment, consisting of interacting atoms, can be quantified through the so-called fragment attributed molecular system energy change (FAMSEC). Here, we report the FAMSEC formalism pertinent for an IQA analysis. The idea of a self and inter-fragment deformation term was also used by Marek *et al.* studying the hydrogen bond[28,29] and applied in comparisons with other decomposition methods like EDA and NOCV[30]. Generalizing the idea of Pendás *et al.*[31], we define the deformation self-energy $\Delta E_{def,self}^{\mathcal{H}}$ of a given fragment $\mathcal{H}$, belonging to a molecule (F) as the difference between the fragment self-energy in the final state E_{self}^{A}, *i.e.* interacting with the other fragments in the molecule F, and the self-energy in the reference state $E_{self,vac}^{A}$, *i.e.* the isolated fragment, but in the very same geometry as in the molecule.

$$\Delta E_{def,self}^{\mathcal{H}} = \sum_{A\in\mathcal{H}} E_{self}^{A} - E_{self,vac}^{A} = \sum_{A\in\mathcal{H}} \Delta E_{self}^{A} \tag{5}$$

The reference electronic state is not constrained to the final one. $\Delta E_{def,self}^{\mathcal{H}}$ (called *promotion energy*) is typically positive (destabilizing) and it accounts for the change of the self-energy of a given fragment. Because of the variation of the intra-fragment interaction E_{int}^{AB}, of a fragment $\mathcal{H}$ composed by one or more atomic basins (A, B $\in \mathcal{H}$), from its reference state $E_{int,vac}^{AB}$, we need a definition of a deformation energy also for this term, $\Delta E_{def,int}^{\mathcal{H}}$.

$$\Delta E_{def,int}^{\mathcal{H}} = \frac{1}{2}\sum_{\substack{\mathrm{A}\neq\mathrm{B} \\ A,B\in\mathcal{H}}} E_{int}^{\mathrm{AB}} - E_{int,vac}^{AB} \tag{6}$$

If a fragment is generated by only one atomic basin, the $\Delta E^{\mathcal{H}}_{def,int}$ will obviously vanish. With $\Delta E^{\mathcal{H}}_{def,self}$ and $\Delta E^{\mathcal{H}}_{def,int}$ it is possible to describe the global intra-fragment energy deformation, but another term is necessary, namely the sum of inter-fragment interactions:

$$E^{frg}_{int} = \frac{1}{2}\sum_{\substack{\mathcal{H}\neq\mathcal{G}\\ \mathcal{H},\mathcal{G}\in \mathrm{F}}} E^{\mathcal{G},\mathcal{H}}_{int} = \frac{1}{2}\sum_{\substack{\mathcal{H}\neq\mathcal{G}\\ \mathcal{H},\mathcal{G}\in \mathrm{F}}} \left(\sum_{A\in\mathcal{H}}\sum_{B\in\mathcal{G}} E^{AB}_{int}\right) \tag{7}$$

$E^{\mathcal{G},\mathcal{H}}_{int}$ is not a deformation energy, as in equations (5) and (6); instead it is total interaction-energy between fragments $\mathcal{G}$ and $\mathcal{H}$. In general, when n fragments are present, E^{frg}_{int} is the sum of $n(n\text{-}1)/2$ interfragment interactions. Coupling equations (7) with (5) and (6), and summing over all the fragments, one obtains the global energy binding contribution ΔE^{frg}_{bind} of many interacting fragment.

$$\Delta E^{frg}_{bind} = E^{frg}_{int} + \sum_{\mathcal{H}}\left(\Delta E^{\mathcal{H}}_{def,self}\right) + \sum_{\mathcal{H}}\left(\Delta E^{\mathcal{H}}_{def,int}\right) \tag{8}$$

In the simple case of only two fragments $(\mathcal{H},\mathcal{G})$:

$$\Delta E^{\mathcal{G},\mathcal{H}}_{int} = \frac{1}{2}\sum_{\substack{\mathrm{A}\neq\mathrm{B}\\ A,B\in\mathrm{F}}} E^{\mathrm{AB}}_{int} - \frac{1}{2}\sum_{\mathcal{H}}\left(\sum_{\substack{\mathrm{A}\neq\mathrm{B}\\ A,B\in\mathcal{H}}} E^{AB}_{int,vac}\right) =$$

$$\frac{1}{2}\sum_{\substack{\mathrm{A}\neq\mathrm{B}\\ A,B\in\mathrm{F}}} E^{\mathrm{AB}}_{int} - \frac{1}{2}\sum_{\substack{\mathrm{A}\neq\mathrm{B}\\ A,B\in\mathcal{H}}} E^{AB}_{int,vac} - \frac{1}{2}\sum_{\substack{\mathrm{A}\neq\mathrm{B}\\ A,B\in\mathcal{G}}} E^{AB}_{int,vac} \tag{9}$$

which takes into account both the intra-fragment and inter-fragment energy contributions, generating a more compact equation for the fragments binding energy:

$$\Delta E_{bind}^{\mathcal{G},\mathcal{H}} = \Delta E_{def,self}^{\mathcal{H}} + \Delta E_{def,self}^{\mathcal{G}} + \Delta E_{int}^{\mathcal{G},\mathcal{H}} \tag{10}$$

According to (3) and using (4), (4a) and (4b), it is possible to decompose the self-energy deformation $\Delta E_{def,self}^{\mathcal{H}}$ and the fragment's interaction-energy $\Delta E_{int}^{\mathcal{G},\mathcal{H}}$ into kinetic and potential energy contributions, in order to gather them together in a more chemical intuitive way:

$$\Delta E_{def,self}^{\mathcal{H}} + \Delta E_{def,self}^{\mathcal{G}} = \sum_{\mathcal{H}} \left(\sum_{A \in \mathcal{H}} \Delta T^{A} + \Delta V_{en}^{AA} + \Delta V_{ee}^{AA} \right)$$

$$= \Delta T_{def}^{\mathcal{H}} + \Delta V_{def,en}^{\mathcal{H}\mathcal{H}} + \Delta V_{def,ee}^{\mathcal{H}\mathcal{H}} + \Delta T_{def}^{\mathcal{G}} + \Delta V_{def,en}^{\mathcal{G}\mathcal{G}} + \Delta V_{def,ee}^{\mathcal{G}\mathcal{G}} \tag{11}$$

$$\Delta V_{def,ee}^{\mathcal{H}\mathcal{H}} = \Delta V_{def,C}^{\mathcal{H}\mathcal{H}} + \Delta V_{def,xc}^{\mathcal{H}\mathcal{H}} \tag{12a}$$

$$\Delta V_{def,ee}^{\mathcal{G}\mathcal{G}} = \Delta V_{def,C}^{\mathcal{G}\mathcal{G}} + \Delta V_{def,xc}^{\mathcal{G}\mathcal{G}} \tag{12b}$$

$$\Delta E_{int}^{\mathcal{G},\mathcal{H}} = \frac{1}{2} \sum_{\substack{\mathrm{A} \neq \mathrm{B} \\ A,B \in \mathrm{F}}} (V_{nn}^{AB} + V_{en}^{AB} + V_{ne}^{AB} + V_{ee}^{AB}) - \sum_{\mathcal{H}} \left(\frac{1}{2} \sum_{\substack{\mathrm{A} \neq \mathrm{B} \\ A,B \in \mathcal{H}}} V_{nn,vac}^{AB} + V_{en,vac}^{AB} + V_{ne,vac}^{AB} + V_{ee,vac}^{AB} \right)$$

$$= \Delta V_{nn}^{\mathcal{G},\mathcal{H}} + \Delta V_{en}^{\mathcal{G},\mathcal{H}} + \Delta V_{ne}^{\mathcal{G},\mathcal{H}} + \Delta V_{ee}^{\mathcal{G},\mathcal{H}} \tag{13}$$

$$\Delta V_{ee}^{\mathcal{G},\mathcal{H}} = \Delta V_{C}^{\mathcal{G},\mathcal{H}} + \Delta V_{xc}^{\mathcal{G},\mathcal{H}} \tag{14}$$

With these equations it is possible to define two main potential energy terms: a classical one $\Delta V_{classic}^{\mathcal{G},\mathcal{H}}$, and a quantum-mechanical one $\Delta V_{xc}^{\mathcal{G},\mathcal{H}}$.

$$\Delta V_{classic}^{\mathcal{G},\mathcal{H}} = \Delta V_{def,en}^{\mathcal{H}\mathcal{H}} + \Delta V_{def,C}^{\mathcal{H}\mathcal{H}} + \Delta V_{def,en}^{\mathcal{G}\mathcal{G}} + \Delta V_{def,C}^{\mathcal{G}\mathcal{G}} + \Delta V_{nn}^{\mathcal{G},\mathcal{H}} + \Delta V_{en}^{\mathcal{G},\mathcal{H}} + \Delta V_{ne}^{\mathcal{G},\mathcal{H}} + \Delta V_{C}^{\mathcal{G},\mathcal{H}} \quad (15)$$

$$\Delta V_{xc}^{\mathcal{G},\mathcal{H}} = \Delta V_{def,xc}^{\mathcal{H}\mathcal{H}} + \Delta V_{def,xc}^{\mathcal{G}\mathcal{G}} + \Delta V_{xc}^{\mathcal{G},\mathcal{H}} \quad (16)$$

Equations (15) and (16), together with the kinetic energy terms, result in the fragments binding energy.

$$\Delta E_{bind}^{\mathcal{G},\mathcal{H}} = \Delta T_{def}^{\mathcal{H}} + \Delta T_{def}^{\mathcal{G}} + \Delta V_{classic}^{\mathcal{G},\mathcal{H}} + \Delta V_{xc}^{\mathcal{G},\mathcal{H}} \quad (17)$$

Which coincides with equations (8) and (10).

Noteworthy, this formalism enables to compare the IQA results with those obtained with energy decomposition analysis (see next paragraph).

2.2.2 Energy Decomposition Analysis

The Energy Decomposition Analysis (EDA) is based on the formalism introduced by Morokuma and Kitaura[19,32] who partitioned the energy of a chemical bond into several contributions. The total bond energy ΔE depends on two major components:

$$\Delta E = \Delta E_{prep} + \Delta E_{int} \quad (18)$$

Where ΔE_{prep} is the energy necessary to promote fragments from their equilibrium geometry and electronic ground state to the geometry and electronic state which they display in the assembled molecule. ΔE_{int} is the interaction energy (or total bonding energy) between two fragments in a molecule which can be further divided as follow:

$$\Delta E_{int} = \Delta E_{els} + \Delta E_{Pauli} + \Delta E_{orb} \quad (19a)$$

$$\Delta E^{\circ} = \Delta E_{els} + \Delta E_{Pauli} \quad (19b)$$

ΔE_{els} is the electrostatic interaction energy between the fragments which are calculated with a frozen electron density distribution in the geometry of the complex. This term is usually attractive. ΔE_{Pauli} gives the destabilizing energy caused by exchange (often called Pauli repulsion), which is calculated when the wave function is orthogonalized and antisymmetrized. ΔE_{els} and ΔE_{Pauli} are frequently summed to give the so-called *steric* term ΔE°, but it should not be confused with the loosely defined steric interaction between substituents in a molecule. The final term ΔE_{orb} gives the stabilization which arises from the orbital interactions when the wave function is fully relaxed. The latter term can be further broken down into orbital contributions with different symmetry.

ΔE_{orb} can be associated with the covalent contributions to the bond and the electrostatic term with the ionic bonding, that means that the ratio between ionic/covalent character of the bond can be obtained. In this way, ΔE_{els} can used to estimate the strength of the electrostatic bonding, while ΔE_{orb} for the covalent bonding[33].

Moreover, from the decomposition analysis above it is possible to extract the energy terms which constitute the total bonding energy ΔE_{int}[34]. Those terms are: the Electrostatic energy, the Kinetic energy, the Coulomb energy and the Exchange-Correlation energy (XC). In order to make a direct comparison

between the EDA and the IQA decomposition methods, we will gather together the Electrostatic and the Coulomb terms in a so called Classic term.

3. EXPERIMENTAL SECTION AND COMPUTATIONAL DETAILS

3.1 Single crystal X-ray diffraction

The single crystal **2a_1** (dimension 0.1, 0.1, 0.2 mm) was collected on a Bruker-APEX-II X-ray diffractometer, using Mo Kα graphite-monochromatized radiation, with generator working at 50 kV and 30 mA. Data were collected at T = 100 K using an Oxford cryosystem series 600; ω-scans of 0.3° were adopted and a total of 5354 frames with exposure times of 40, 80 and 120 seconds were collected. The data were integrated using SAINT (version V7.23A[35]), and corrected analytically for absorption and empirically (with SADABS[36]) for the other anisotropies of the diffraction.

The single crystal **2a_2** was mounted on an Agilent SuperNova diffractometer, equipped with a MoKα microsouce (50 kV and 0.8 mA), Al-filtered[37]. Data were collected at T = 110 K using an Oxford cryosystem 700, with ω-scans of 1.0° were adopted and a total of 4282 frames with exposure times of 20, 30 and 120 seconds were collected. The software CrysAlisPro Version 1.171.37.35g[38], was used to perform data collection and reduction. Data were corrected for absorption (analytically) and diffraction anisotropies using ABSPACK[38] routine of Crysalis.

More information about the two experiments are reported in Table1.

Table 1. Crystallographic Data and Structure Refinement Parameter for 2a_1 and 2a_2

Identification code	α-**2a_1**	α-**2a_2**
Empirical formula	C_{40} H_{20} Co_6 O_{16} P_2	C_{40} H_{20} Co_6 O_{16} P_2
Formula weight	1172.08	1172.08
Temperature	100 K	110 K
Wavelength	0.71073	0.71073
Crystal system	Monoclinic	Monoclinic
Space group	$P2_1/c$	$P2_1/c$
a/Å	10.0109(4)	10.0180(1)
b/Å	20.8610(8)	20.8737(1)
c/Å	20.4255(8)	20.4382(1)
β/°	92.176(2)	92.1609(4)
V/Å^3	4262.5(3)	4270.85(5)
Z, Calculated density /Mg m^{-3}	4, 1.826	4, 1.823
Absorption coefficient /mm^{-1}	2.428	2.423
Θ-range/°	1.952 to 45.294	1.951 to 45.506
Reflections collected/unique	121109 / 32541	329282 / 36061
R_{merge}	0.0345	0.0461
R_{rim}	0.0403	0.0488
Multiplicity (inf-0.5 Å)	3.7	9.1
Multiplicity (inf-0.7 Å)	7.0	12.1
Spherical Atom Refinement		
Data / restraints / parameters	32541 / 0 / 577	36061 / 0 / 577
Goodness-of-fit (F^2)	1.003	1.028
R_1, wR_2 [$I > 2\sigma(I)$]	0.0382, 0.0704	0.0296, 0.0678
R_1, wR_2 (all data)	0.0784, 0.0812	0.0450, 0.0736
Multipolar Refinement		
Data / restraints / parameters	21540 / 0 / 1917	28825 / 0 / 1917
Goodness-of-fit (F^2)	1.1405	1.2502
R_1, wR_2 [$I > 2\sigma(I)$]	0.0289, 0.0407	0.0211, 0.0500
R_1 (all data)	0.0393	0.0233

3.1.1 Multipolar expansion

In Table 1, we report the results of conventional and multipolar refinements for the salt $[Co_6P(CO)_{16}]^-$ $[PPh_4]^+$ (**2a_1, 2a_2**), carried out with ShelX[39,40] and XD[41] programs, respectively (Table 1). The multipolar refinement was carried out using data with $I > 2\sigma(I)$, using the Hansen and Coppens model, as showed in equation (2). For Co and P atoms, the multipolar expansion was truncated at the hexadecapole level, for O and C at the octupole level. The scattering factors of cobalt atoms was constructed from the $4s^2 3d^7$ configuration of the isolated atom, but the population of the 4s valence orbitals was not refined and all the deformation density of Co atoms was constructed from 3d orbitals for all atoms. The Volkov and Macchi atomic functions[42] were employed to describe the radial densities of all atoms. The positions of H atoms were kept fixed at a C-H distance equal to 1.079 Å, according to average neutron diffraction data for tetraphenylphosphonium cation. The H thermal motion was considered isotropic and only the monopole and the C-H oriented dipole parameters were refined. Expansion/contraction parameters κ and κ' were refined for each kind of element: two different sets were assigned to phosphorus (to discriminate the phosphide from the phosphonium atoms) and carbon (to distinguish carbonyl carbons and phenyl carbons). For all expansion/contraction parameters, κ' were constrained to κ, in order to avoid divergence of the refinement. For hydrogen atoms, κ and κ' were kept equal to the standard value of 1.2. Third- and fourth-Gram-Charlier coefficients of anharmonicity (Table S2) were refined for Co and P (phosphide) atoms. The residual distribution and normal probability plots of diffraction intensities discrepancies and other parameters are reported in Supporting Information Figures S1- S3 and Tables S1-S3.

The two experimental charge densities of the anion $[Co_6P(CO)_{16}]^-$ were analyzed using the QTAIM routine implemented in the module XDPROP. In Figure 1 and Table S4 we report the main topological indices, the charges of the semi-interstitial atom Q(X). The Lagrangian function integrated within an

atomic basin, $L(\Omega)$, should vanish and therefore it is an indicator of accuracy of the integration. With our models, for P atom this value resulted equal to $-2.01\cdot10^{-3}$ au in **2a_1** and $-3.83\cdot10^{-3}$ au in **2a_2**, for metal atoms, from Co1 to Co6 respectively, $L(\Omega)$ values resulted $1.52\cdot10^{-2}$, $1.62\cdot10^{-2}$, $2.74\cdot10^{-2}$, $4.38\cdot10^{-2}$, $1.15\cdot10^{-1}$ and $1.22\cdot10^{-1}$ au in **2a_1** and $-2.72\cdot10^{-4}$, $1.10\cdot10^{-3}$, $2.22\cdot10^{-2}$, $1.74\cdot10^{-2}$, $1.03\cdot10^{-1}$, $2.83\cdot10^{-2}$ au in **2a_2**.

3.2 Computational Details

EDA: DFT calculations have been performed with the program package ADF2014[43], using the functional B3LYP and the triple zeta with double polarization functions (TZ2P) Slater type orbitals (STOs) as basis functions for the SCF calculations. . All the structures have been optimized and verified as minima on the potential energy surface by calculation of the vibrational frequencies.

QTAIM/IQA: The program package AIMALL was used. The wave functions were calculated with Gaussian09 [44], using the B3LYP functional and *correlation-consistent* triple zeta (cc-PVTZ) basis set. B3LYP is one of the few DFT models supported by AIMALL for the correct evaluation V_{xc}^{AB} in the IQA analysis[45]. The molecular geometries were optimized and the nature of the minima have been verified by calculation of the vibrational frequencies.

Wiberg bond indices: they were computed on the B3LYP/cc-PVTZ optimized geometries using the NBO3.1 program linked to Gaussian09.

4. RESULTS AND DISCUSSIONS

4.1 The molecular structures and the crystal packing

As we reported in a previous work,[9] the salt $[Co_6As(CO)_{16}]^-[PPh_4]^+$ (**1**[PPh_4]) is known in two different conformational polymorphs, **α-1a**[PPh_4] and **β-1b**[PPh_4]. The solid state form α (space group, $P2_1/c$) is

similar for **1a** and **2a** (*i.e.* $[Co_6P(CO)_{16}]^-[PPh_4]^+$, [6]), whereas the form β (space group, Pbca) has been observed for **1b** only and never obtained for the phosphide analogue.

Both anionic isomers feature a cluster cage (an 'unfolded' octahedron), made of a folded chain of four edge-sharing triangles surrounding a "semi-interstitial" heteroatom. The idealized symmetry is C_2, with the two-fold axis going through the heteroatom and the midpoint of the Co1-Co2 edge. The most striking difference between the isomers **a** and **b** is the Co1-Co2 distance, which is shorter for **a** (2.944(1) in **1a**, 2.935(2) Å in **2a**) and longer for **b** (3.457(2) Å in **1b**). Theoretical calculations predict that in gas phase and in solution the isomers of type **b** would be the most stable forms for the $[Co_6X(CO)_{16}]^-$ anions. In the solid state, however, polymorphs type α (hence, the isomers type **a**) have a much more efficient type of packing, as revealed by the mass densities of the arsenides polymorphs (1.812 for α-**1a** and 1.758 g/cm^{-3} for β-**1b**). The quality of the crystal samples is also much better for the α-**1b** polymorph, compared to β-**1b**; this may be an indication (together with the higher density of α-**1a** and the missing β-**2b**) of β-type polymorphs being only kinetic products, not always isolable. The higher quality of samples α-**2a** enabled us to carry out extensive data collections with the purpose of an experimental determination of the charge density, not possible for α-1**a** or β-**1b**. For sake of improving the precision of the measured quantities, two different crystals of $[Co_6P(CO)_{16}]^-[PPh_4]^+$ (Table 1), hereinafter **2a_1** and **2a_2**, respectively, were measured. The two structure determinations (all carried out at low T) provide very similar values of the "critical" Co1-Co2 distance, namely 2.8901(2) Å for **2a_1** and 2.8922(1) Å for **2a_2** (from spherical atom refinement), but they significantly differ from the characterization by *Chini et al.*[6], carried out at room temperature, 2.935(2) Å. Indeed, multi temperature diffraction shows that Co1-Co2 is quite flexible and it significantly contract as the sample is cooled.

4.2 Charge Density Analysis

QTAIM enable to gain, from the electron density distribution only, important insight into the nature of the chemical bonding, which is especially useful when dealing with non-standard kind of bonding, especially metal-metal bonding and metal-interstitial atoms bonding[14], both present in species **1** and **2**. As anticipated, the crystal sample quality enabled the experimental determination only for isomer **2a**, whereas **1a**, **1b** and, obviously, the elusive **2b** are determined only by theoretical simulations.

In Figure 1, we report the topological indices for the main interactions in the anionic clusters. This enables a comparison between the two kinds of isomers (**a** vs **b**) and the two kinds of semi-interstitial atoms (P vs. As). From theoretical calculations, one may also obtain quantities related to the electron pair distribution, as for example the electron delocalization indices[46,47] that are very useful, especially to characterize the electron-donor ability of interstitial atoms. In keeping with all bridged metal-metal bonds[48], the molecular graphs of all clusters lack of direct Co-Co bond paths, with the exception of Co1-Co3 (and the symmetry equivalent Co2-Co4) in **1b**. If optimized with the basis set 6-311+G(d,p), **1a** also features the same bond path, although with almost overlapping bond and ring critical points. As we previously discussed for carbonyl bridges, the lack of a bond path does not necessarily imply the absence of a Co---Co interaction, but simply the dominance of the *through-bond* interaction over the direct *through-space* one.[49] Therefore, the main feature of the molecular graphs is the connection of all Co atoms to the semi-interstitial atom. Given the C_2 symmetry of the gas phase molecules and the pseudo-symmetry in the solid state, the Co-X paths can be grouped into three symmetry independent interactions, namely to Co1 (= Co2), Co3 (= Co4) and Co5 (= Co6) (Figure 1,2).

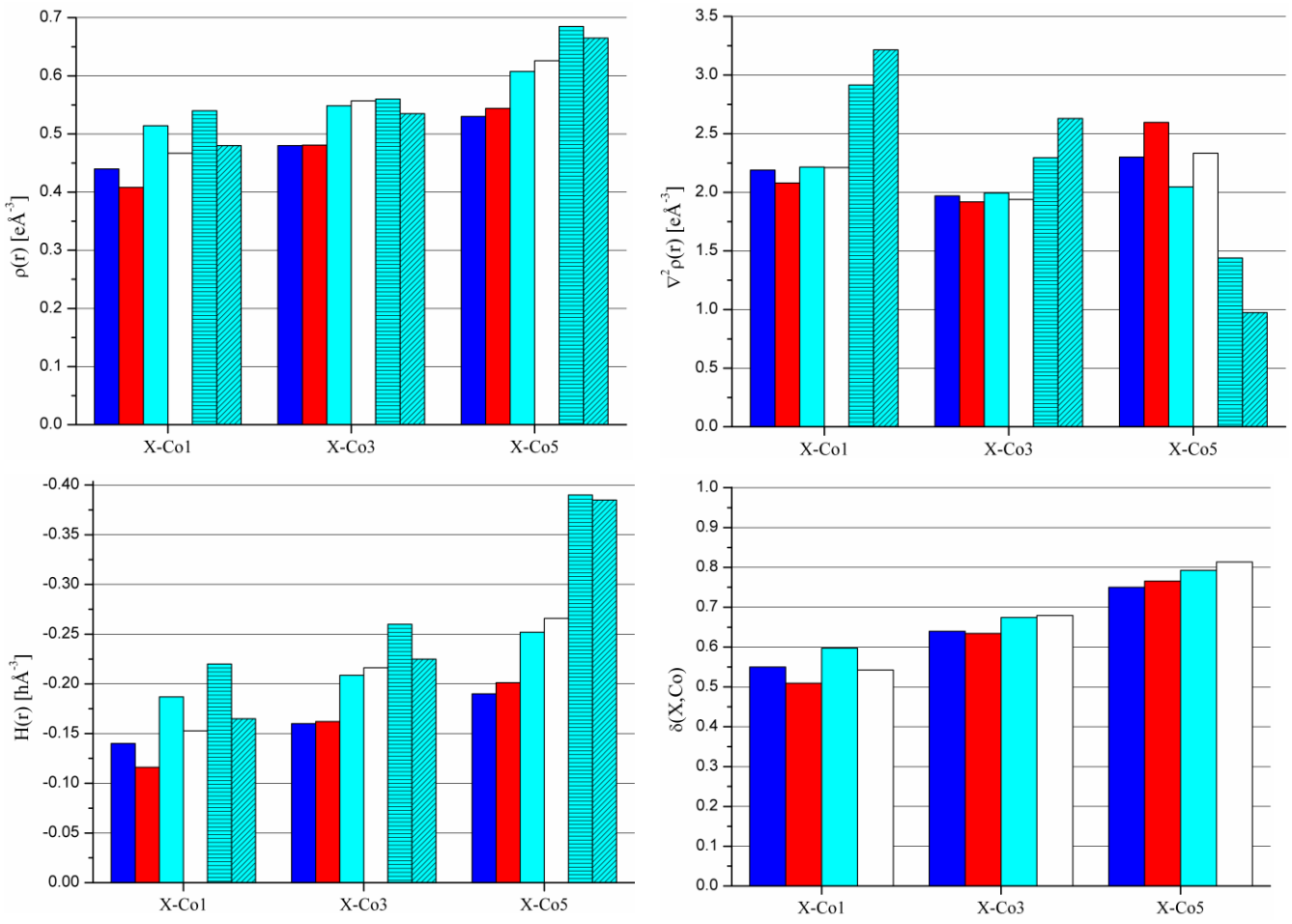

Figure 1. Results of the Theoretical and Experimental Topological Analysis. Theoretical calculations refer to the point group symmetry C_2, meaning that X-Co1 = X-Co2, X-Co3 = X-Co4, X-Co5 = X-Co6, Co1-Co3 = Co2-Co4. Theoretical values of $\int_{A\cap B}\rho(r)$ are reported in Table S4. Experimental values of $Q(Co_n)$ and $\delta(Co_n,Co_m)$ are reported in Table S5. **1a**= Blue; **1b**=Red; **2a**=Cyan; **2b**= White. α-**2a_1,2** = Cyan -weft (**1**= horizontal strings, **2**= diagonal strings).

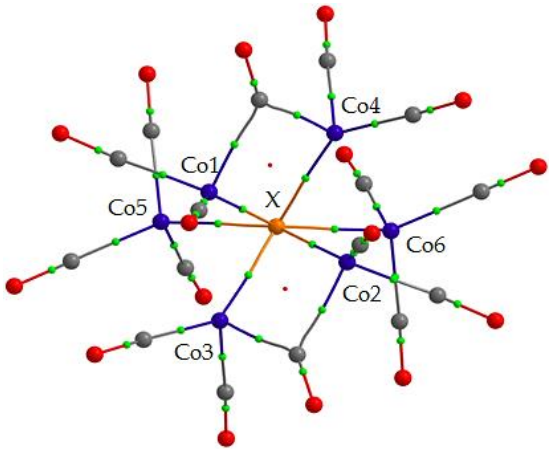

Figure 2. Molecular graph of the system $[Co_6X(CO)_{16}]^-$ (for type-**a** conformer**)**.

From the calculated and experimental molecular graphs (Figure1, Table S4), Co-X interactions are in general quite strong, because they feature a relatively large amount of electron density at the bond critical points, significantly negative values of the energy density, low values of the kinetic energy density and large electron delocalization indices. A *caveat* is necessary, thought, because the valence shell electrons of the metals are shared among all 6 Co atoms, which implies only a much smaller amount of electron pair delocalization per each Co-Co interaction. The main differences between X= P and X = As are the larger negative charge of P and the larger delocalization of the electrons in Co-P bonds. The theoretical charges are in agreement with the experimental values for **2a**, in both samples we measured (see Table S4, S5). On the other hand, it seems that the type of isomer does not affect so significantly the charge of the main group atom, despite the rather different set of Co-X bonds.

Given the absence of direct Co-Co bond paths (apart from **1b**), only delocalization indices can shed light on these interactions (Table S5). The electron sharing between Co atoms is in general slightly weaker than with the semi-interstitial atoms (Figure 1), in keeping with general trends of bridged metal-metal

interactions [14]. In addition, Co1-Co4 (equivalent to Co2-Co3), which is also supported by a carbonyl bridge, is even weaker with an electron sharing down to less than 0.3 pairs.

Given the rather distorted nature of the Co cages in both kinds of isomers, it is very important to characterize the hybridization state of the interstitial atoms. From electron density distribution, this can be achieved through the analysis of the Laplacian distribution within the atomic basin. In fact, $L(\mathbf{r}) = -\nabla^2\rho(\mathbf{r})$, has been widely used to characterize electron pair distribution and therefore atomic hybridization and interatomic interactions, because the Laplacian enhances the features of the charge distribution and the electron pair localization. *Valence shell charge concentrations* (VSCC), *i.e.* (3,+3) critical points of $L(\mathbf{r})$, for the semi-interstitial atoms have been searched and located both theoretically and experimentally, Figure 3. All values are reported in Table S6.

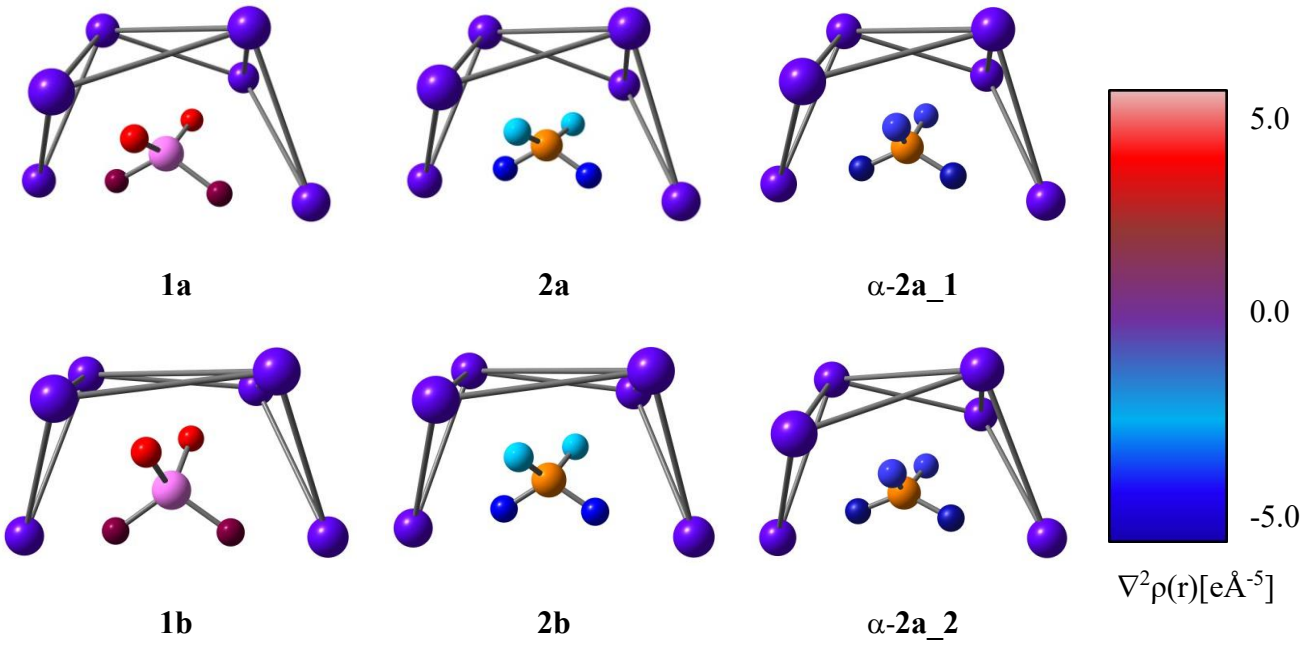

Figure 3. Experimental and Theoretical Atomic Graph of P and As atom. Color coding follows the $\nabla^2\rho(\mathbf{r})$ [e Å^{-5}] scale on the right.

The distribution and the number of VSCCs reflects the stereochemistry of an atom, better than its connectivity. In fact, the bonds to a given atom may be elusive or differ in nature and therefore not usable to ascertain the hybridization state. Here, this is very important for the semi-interstitial atoms. From the theoretical calculations, P features four VSCC's in the third (valence) shell suggesting a distorted tetrahedral coordination. Similarly, in the fourth shell, As has four maxima at $L(\mathbf{r}) < 0$. Strictly speaking, they are not charge concentrations. However, one should take into account that, even in the isolated atom, As has a vanishing maximum of the spherically averaged Laplacian in the fourth shell, which occurs at $L(\mathbf{r}) < 0$[50]. Thus the local maxima in the fourth shell, albeit with $L(\mathbf{r}) < 0$, can be taken as representative of the valence orbital state of As, as they are for P. Both VSCC's distributions (and especially for X = P) clearly differ from what expected with the geometrical hexa-coordination of the semi-interstitial atoms. In **2a** and **2b**, the maxima are directed towards Co3, Co4, Co5 and Co6, with uneven values of $\rho(\mathbf{r})$ and $\nabla^2\rho(\mathbf{r})$ (Table S6), bringing a higher charge concentration to Co5 and Co6, which increases going from **2a** to **2b**. Analogously, the four maxima in **1a** and **1b** point towards Co3, Co4, Co5 and Co6, with a trend in the Laplacian values that reflects the behavior of $\nabla^2\rho(\mathbf{r})$ in the phosphide isomers (*i.e.* more negative towards Co5 and Co6). Thus, in keeping with distances and electron density sharing, the interaction of the interstitial atom is stronger with the two Co atoms for which the hypothetical edge of an octahedron is clearly broken (Co5-Co6 is in excess of 4 Å in all isomers). Instead, the interactions with the two atoms involved in the short or long Co-Co bond (*i.e.* Co1, Co2) are anyway weak in both isomers. So weak, that the atomic graph of P does not show any charge localization in that direction.

The experimental atomic graphs are in good agreement with the theoretical values. In both cases, there are four charge concentrations. Together with the distances of the critical points from the P nucleus and $\nabla^2\rho(r)$ values (Table S6), this confirm the computational prediction. Therefore, when X = P, one can speak

of a distorted tetrahedral stereochemistry for the interstitial atom, better than a distorted octahedral one. Although weaker, and based on theoretical calculations only, the same conclusion holds for the As clusters.

4.3 Energy breakdown

While the charge density partition inform on the hybridization states, and could take advantage of experimental confirmation, even more insight could be obtained from an energy decomposition. Despite the total energy is also an expectation value (of the Hamilton operator), it is not really an observable and cannot be partitioned from any experimental measure.

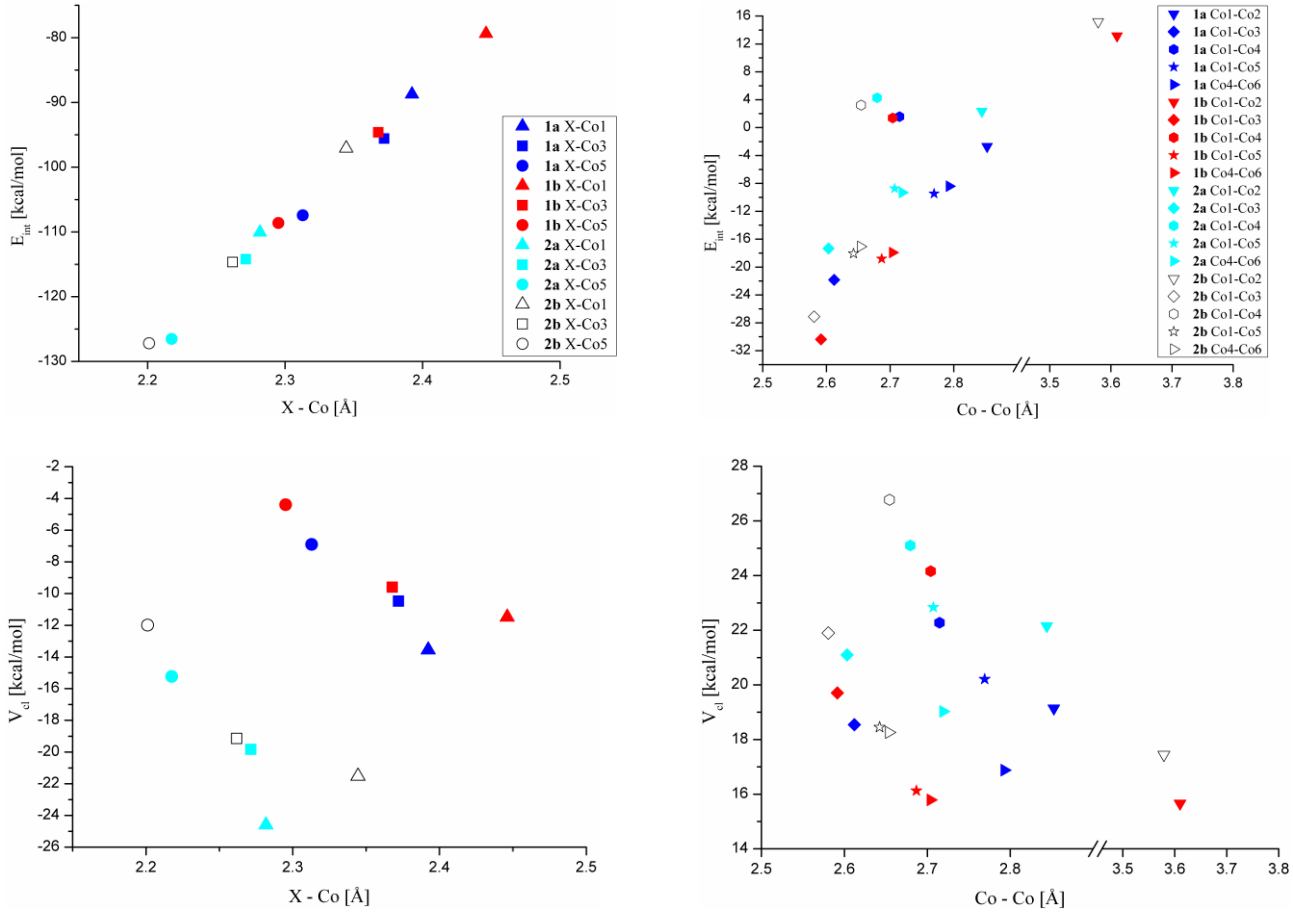

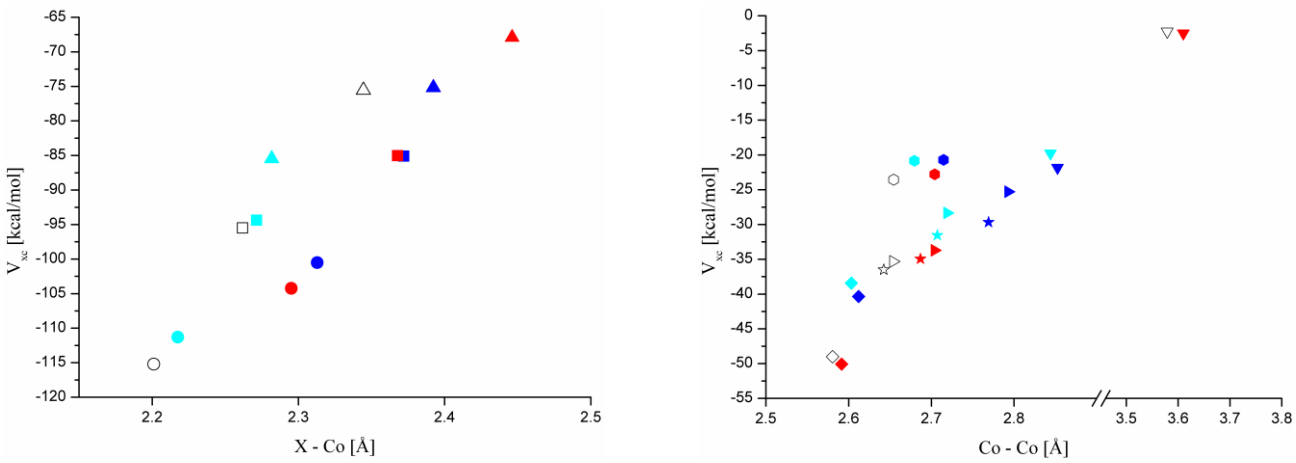

Figure 4. Interaction Energy E_{int}^{AB}, classic term V_{cl}^{AB} and exchange-correlations term V_{xc}^{AB} from IQA decomposition; **1a**= Blue; **1b**=Red; **2a**=Cyan; **2b**= White; The terms for Co1-Co2 of **1b** and **2b** have been omitted because the long distance produced too weak interactions.

Therefore, for this analysis we rely only on theoretical values and we present here two kinds of analysis, the interacting quantum atom (where the charge density is used to define the atomic basins) and the energy decomposition analysis (where atoms are pre-defined by their atomic basis sets).

4.3.1 Interacting Quantum Atoms

The IQA energy terms are reported in Figure 4 and Table S7. The interaction energies between semi-interstitial atoms and Co atoms are always larger than the Co-Co ones. Of course, this is favored by the cooperation between the electron-sharing (exchange) and the columbic term. For Co-X, both are favorable, at variance from Co-Co, that are of course associated with strongly destabilizing columbic terms. Nevertheless, the exchange is quite large and clearly dominating, confirming that the X-Co strength decreases along the series X-Co5 > X-Co3 > X-Co1. The trend is more pronounced for the **b** isomers. The P atom gives rise not only to a larger orbital overlap with the metal atoms (Table S7; see in particular the high values of V_{xc}^{AB}), but also to a stronger electrostatic interaction, V_{cl}^{AB}, caused by its more negative

charge. Overall, the interaction of P with the cage is stronger than that of As, in terms of both covalency and ionicity. The higher ratio between covalency and ionicity for X=As is simply due to the lower negative charge of As and it should not be misinterpreted. Indeed, an interaction like Co-P can be simultaneously more covalent and more electrostatic[51] (Table S7). On going from **a** to **b,** V_{xc}^{AB} becomes more negative for X-Co5, whereas X-Co3 remains almost constant and X-Co1 becomes more positive. The classical potential energy V_{cl}^{AB} doesn't follow the same trend, in fact it always increases from **a** to **b**, particularly for X-Co1 and X-Co5.

The energy decomposition of the Co-Co bonds show that they are dominated by the exchange-correlation interaction, as expected for metal-metal bonds[52]. The strongest interaction is Co1-Co3, though highly dependent on both the cage conformation and the semi-interstitial atom. The interactions of Co1 with Co4 and Co5 depend mainly on the conformation of the cluster and Co1-Co4, which is bridged by a carbonyl, is poorly stabilizing or even destabilizing. Co1-Co2 has a considerable elongation on going from isomers **a** to **b**, producing a large difference in the interaction energy. Even if V_{xc}^{AB} has almost the same value for the two semi-interstitial atoms, V_{cl}^{AB} is much more destabilizing in the phosphide clusters. An overall stabilizing energy for this interaction (Table S7) was found only for **1a**. As expected, Co4-Co6 is similar to Co1-Co5 but weaker, except for **2a**.

The most evident change due to the isomerization is the elongation (or shortening) of Co1-Co2. However, less evident are the changes of the other interactions. We can pinpoint the following correlation: the longer is Co1-Co2, the weaker becomes X-Co1 (=X-Co2), whereas, as reported in Figure 4, E_{int}^{AB} of Co1-Co3 (Co2-Co4) increases in modulus. The above discussed trends are confirmed also by the Wiberg indices, see Table 2.

Table 2. Wiberg Bond Index of X-Co and Co-Co

	X-Co1	X-Co3	X-Co5	Total WBI (X)	Co1-Co2	Co1-Co3	Co1-Co4	Co1-Co5	Co4-Co6
1a	0.456	0.524	0.671	3.998	0.190	0.309	0.234	0.320	0.202
1b	0.408	0.530	0.712	3.961	0.063	0.441	0.241	0.294	0.273
2a	0.484	0.537	0.669	4.075	0.173	0.298	0.224	0.329	0.222
2b	0.428	0.553	0.708	4.047	0.053	0.437	0.232	0.303	0.282

The total WBI values for the semi-interstitial atoms are almost constant in all isomers but the individual interactions have different strength. The WBI reflects also what it was obtained in the atomic graph analysis: the values of X-Co5 are the largest and very similar in all the isomers. **2b** has the highest value of X-Co3, which is quite close X-Co5, and a much lower value of X-Co1, in agreement with the previously discussed tetracoordination. Bond index for Co1-Co3 features the very same value for both **1b** and **2b**, meaning that also for the phosphide isomer the presence of a metal-metal interaction cannot be not excluded. All the other Co-Co indexes follow the trend outlined by the IQA analysis, in particular in the low sensitive values for Co4 and Co5, but also in the behavior with Co2.

4.3.2 Energy Decomposition and Fragment Interaction Analysis

The traditional EDA implies the definition of two closed- or open-shell fragments, whose interaction is evaluated in terms of the classical Morokuma's scheme[32]. The identification of the fragments and the assignment of their electronic configuration are essential and may bias the interpretation.[34,53] The atomic charges, the stereochemistries and the stability of known metal clusters, imply that the fragments to consider are $^{1}X^{-1}$ and $[Co_6(CO)_{16}]^0$. ΔE_{prep} implies a) the excitation of the semi-interstitial atom (X^{-1}) from its ground state triplet to the singlet excited state and b) the deformation of the $Co_6(CO)_{16}$[54] cluster geometry to produce the distorted geometries of **a** and **b** (See Table 3).

Table 3. Preparation Energies [kcal/mol] for the cluster $[Co_6X(CO)_{16}]^-$

	$^3X^{-1} \rightarrow {}^1X^{-1}$	$Co_6(CO)_{16} \rightarrow [Co_6(CO)_{16}]^0$(**a**)	$Co_6(CO)_{16} \rightarrow [Co_6(CO)_{16}]^0$(**b**)
ΔE_{prep}(P)	26.9	103.7	113.4
ΔE_{prep}(As)	24.3	111.9	116.7

The deformation necessary to reach conformation **a** is less energy demanding than for **b**. In the phosphide isomers, this difference is even larger because of the smaller (Pauli) repulsion occurring in **a** (see Figure 5). The ionic radius of As^{-1} is so large that the energy required to form either **a**- or **b**-shape metal cages differs by less than 5 kcal/mol.

In Table 4, we compare the "classical" partitions for EDA and IQA, reporting the terms from equation (19a) and (10), respectively. For the fragment partition, and in particular for the reference fragments, the very same scheme used for the calculation of ΔE_{int} in EDA was used for IQA, *i.e.*, the semi-interstitial atom in the electronic state $^1X^{-1}$ as one fragment and the cage $[Co_6(CO)_{16}]^0$ presenting the same geometry in the final molecule as second fragment. Moreover, we carried out a so called "Energy Terms Partition", which in the case of EDA it is automatically done during the bond energy decomposition by ADF; for IQA, we adopted the formalism presented in the introduction (equation (17)).

ΔE_{els} and ΔE_{orb}, both stabilizing, are larger for isomers **a**, particularly X = P. The ΔE_{Pauli} term addresses isomers phosphide isomers as less stable and conformer **a** as less stable than **b**.

According to Hopffgarten and Frenking[17], ΔE_{els} could be used to estimate the degree of electrostatic character of a bond (which not necessarily coincides with the ionicity), whereas ΔE_{orb} would represent the covalent character. The electrostatic term slightly overwhelms the orbitalic one (55%:45% for the arsenides, 53%:47% for the phosphides). For a deeper understanding of the X−cage bond, in Table S8 an

analysis is reported of the main contribution to the orbital interaction provided by the valence orbitals of the semi-interstitial atom.

Table 4. EDA/IQA Classical and Energetic Components Partition [kcal/mol] of $^{1}X^{-1}$ + $[Co_6(CO)_{16}]^0$

	EDA					IQA			
	1a	**1b**	**2a**	**2b**		**1a**	**1b**	**2a**	**2b**
				Classical Partition					
ΔE_{pauli}	1313.2	1219.8	1415.5	1317.4	$\Delta E^{\mathcal{H}}_{def,self}$	329.0	245.6	311.0	336.4
ΔE_{els}	-882.3	-835.4	-915.2	-872	$\Delta E^{\mathcal{G},\mathcal{H}}_{int}$	-607.5	-531.6	-611.3	-647.5
ΔE_{steric}	430.8	384.4	500.2	445.4	$\Delta E^{\mathcal{G},\mathcal{H}}_{bind}$	-278.5	-285.9	-300.3	-311.1
ΔE_{orb}	-716.3	-676.5	-804.4	-761.1					
ΔE_{int}	-285.5	-292.2	-304.2	-315.7					
$\%\Delta E_{els}$	55.2	55.3	53.2	53.4					
$\%\Delta E_{orb}$	44.8	44.7	46.8	46.6					
				Energy Terms Partition					
Classic	-569.1	-566.4	-599.4	-593.4	Classic	-452.6	-476.7	-611.9	-622
Electrostatic	-882.3	-835.4	-915.2	-872					
Coulomb	313.2	269	315.9	278.6					
XC	-385.3	-355.1	-404.7	-373	XC	-331.5	-302.8	-334.4	-302.7
Kinetic	668.9	629.4	700	650.6	Kinetic	505.6	493.6	646.1	613.5
%Classic	59.6	61.5	59.7	61.4	%Classic	57.7	61.2	64.7	67.3
%XC	40.4	38.5	40.3	38.6	%XC	42.3	38.8	35.3	32.7

$\Delta E^{\mathcal{H}}_{def,self}$ is positive and describes the energetic deformation of a fragment upon the molecular formation[31]. The stabilizing contribution $\Delta E^{\mathcal{G},\mathcal{H}}_{int}$, on the other hand, is indicative of the constructive interaction between the fragments $^{1}X^{-1}$ and $[Co_6(CO)_{16}]^0$. $\Delta E^{\mathcal{H}}_{def,self}$ follows the same trend of ΔE_{Pauli} and ΔE_{steric} for the isomers **1a** and **1b**, meanwhile for **2a** and **2b** it produces very similar values, slightly more destabilizing for the open isomer. The same behavior is seen again for $\Delta E^{\mathcal{G},\mathcal{H}}_{int}$ *i.e.*, **1a** is more stabilized than **1b**, and the opposite for the phosphides isomers. ΔE_{int} and $\Delta E^{\mathcal{G},\mathcal{H}}_{bind}$, on the other hand, are very well in agreement, with a difference of just few kcal/mol, this result tells us that both the partition methods and bonding analysis produce the same total bonding energy for interacting fragments. Moreover, now the trends are in perfect agreement, producing higher (more stabilizing) bonding energy for open isomers **b**, in favor of X=P. Energy terms partition produced interesting results. By isolating the Classic, Kinetic and XC term from both ΔE_{int} and $\Delta E^{\mathcal{G},\mathcal{H}}_{bind}$ it emerges that proportions and trends are the very same.

Quantitatively, EDA produces higher absolute values compared to IQA. However, the ratio between Classic and XC energies of the two decomposition methods are very similar. The Classic term clearly overwhelms the XC (ca. 60% *vs*. 40%), in particular for **b** isomers. In EDA, no difference appears on moving from As to P, whereas in IQA the Classic term is clearly larger, in percentage, for P isomers. This may strongly depend on the definition of the atomic charges, and the fact that in IQA they are not predetermined.

According to the above bonding analysis, we can confirm that, even if the individual X-Co interaction is mainly covalent, the energy that keeps together the metal-carbonyl cage with pnictogen semi-interstitial atoms (P,As) has a more electrostatic nature. In other words, the interaction between the carbonyls and the interstitial atoms plays an important role, although invisible in the charge density.

In Figure 5, we report the ΔE_{prep} and ΔE_{int} terms of the energy decomposition for the fragments $^{1}X^{-1}$ and $[Co_6(CO)_{16}]^0$ (see also Table 3 and 4) and the total bonding energy ΔE (see also Table S9. The trend followed by ΔE is the same of ΔE_{int}, confirming that the most stabilized species are the **b** isomers and that P has the strongest binding. Even if isomers **a** produce the most stabilizing contributions of ΔE_{els} and ΔE_{orb}, the higher destabilization of the Pauli term inverts this trend, and **b** results as the most stable conformation (in isolation).

For the phosphides the effect of the cage's conformation is much more relevant that for the arsenides (Figure 5), because of both the destabilizing (ΔE_{prep}) and stabilizing (ΔE_{int}) contribution. All these mechanisms are anyhow "hidden" in the final energy difference (ΔΔE), due to mutual cancellation. ΔΔE results to be the very same for **1** and **2**, meaning that even if there is an energy difference between isomers of the same chemical nature (same semi-interstitial atom)[9], the preparation energy has the effect of cancelling this discrepancy. If this is correct, the hypothesis of the existence of **2b**, at least in solution, is reinforced, although its isolation may not be possible and so far, despite our repeated attempts, has always failed.

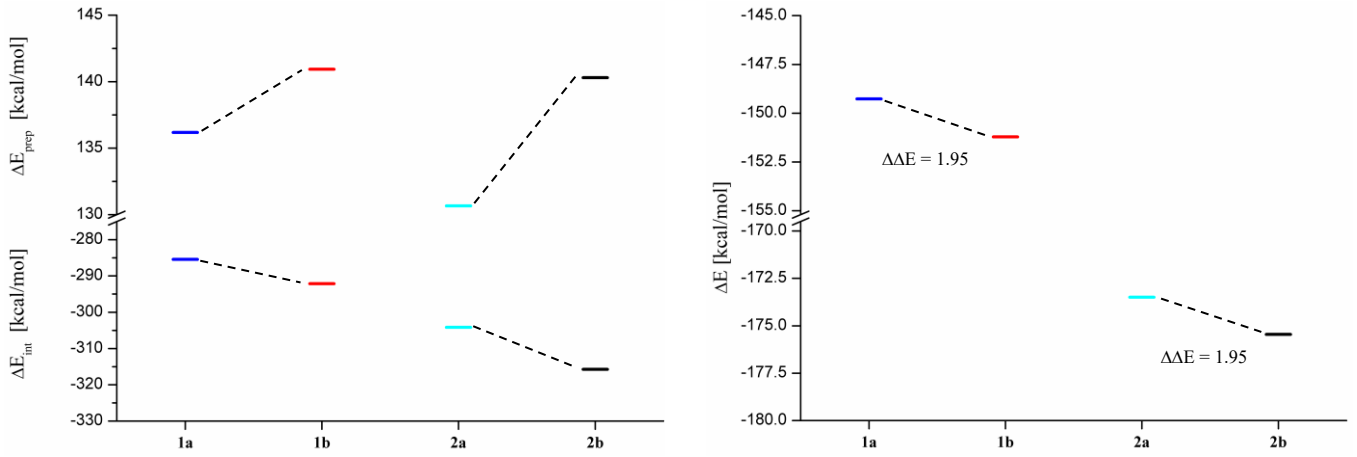

Figure 5. ΔE_{prep}, ΔE_{int} (left), the total bonding energy ΔE (right); **1a**= Blue; **1b**=Red; **2a**=Cyan; **2b**= Black. ΔΔE are the total bonding energy differences.

5. CONCLUSIONS

In this work, we have analyzed the chemical bonding in high nuclearity transition metal carbonyl clusters with semi-interstitial main group atoms, focusing on the species $[Co_6X(CO)_{16}]^-$. The study involved both charge density and energy partitioning, adopted to characterize the ratios between covalent and electrostatic terms of the interactions, the hybridization and oxidation states of the main group atoms and the behavior of two seminterstitial atoms of the same group (namely P and As). The stereochemistry of the clusters under investigation is quite peculiar, because of the two possible conformers that differ mainly in the distortion of the metal cages (and corresponding conformation of CO ligands). The charge density analysis revealed the larger atomic charge of the phosphide compared to the arsenide, anyway smaller than the formal oxidation state of -1. The stronger electrostatic interactions of the phosphide derivative does not hamper a larger covalency of the P-Co interactions, compared to the As-Co ones, which is addressed both by charge and energy partition methods. The hybridization of the semi-interstitial atom remains sp^3-like in the phosphide and in the arsenide. Co-Co interactions are globally quite weak, even if the electronic exchange and the energy stabilization in Co1-Co3 (= Co2-Co4) interactions is enough to produce a bond critical point of the theoretical electron density distribution of **1b**, the overall structure is supported mainly by the more robust X-Co bonds, which according to IQA partition have quite larger interaction energies and bond orders.

EDA and IQA agree in finding the interaction between the semi-interstitial atoms and the overall cages mainly electrostatic, although Co-X interactions, alone, are mainly shared interactions.

For one of the species, $[Co_6P(CO)_{16}]^-[PPh_4]^+$ α-**2a**, the accurate low temperature X-ray diffraction was measured on different crystal samples, in order to obtain an experimental charge density to be compared with the theoretical ones, calculated for all the four $[Co_6X(CO)_{16}]^-$ (X=As,P) isomers. This study is the first comprehensive analysis of chemical bonding in these species, merging the complementary viewpoints of

energy and charge density partitioning in order to gain insight into the stereochemistry of these clusters. This enabled to pinpoint the role and the stereochemistry of the main group semi-interstitial atoms.

Having produced a solid theoretical framework to analyze these species, we plan to extend out investigations other higher nuclearity clusters featuring interstitial or semi-interstitial main group atoms, with the purpose of obtaining a comprehensive view of the chemical bonding in this class of molecules.

ASSOCIATED CONTENT

SUPPORTING INFORMATION

In the Supporting Information file, we report distribution of residual densities, normal probability plots, experimental bond lengths, topological analysis of the electron density and of the Laplacian, IQA individual bond energies, stabilization and bonding energies, gas phase calculated geometries and IR spectra. Crystallographic information files for **2a_1** and **2a_2** are deposited at the Cambridge Structural Database (CCDC 1824286-1824287).

AUTHOR INFORMATION

Corresponding Authors

E-mail: piero.macchi@dcb.unibe.ch

ACKNOWLEDGEMENTS

We thank the Swiss National Science Foundation (Project Nr. 160157) for the financial support.

REFERENCES

(1) Chini, P. A New Cluster Carbonylcobaltate. *Chem. Commun.* **1967**, 29.

(2) Braye, E.; Dahl, L.; Hubel, W.; Wampler, D. L. The Preparation, Properties and Structure of the Iron Carbonyl Carbide $Fe_5(CO)_{15}C$. *J. Am. Chem. Soc.* **1962**, *84*, 4633–4638.

(3) Vidal, J. L.; Walker, W. E.; Pruett, R. L.; Schoening, R. C. $[Rh_9P(CO)_{21}]^{2-}$. Example of Encapsulation of Phosphorus by Transition-Metal-Carbonyl Clusters. *Inorg. Chem.* **1979**, *18*, 129–136.

(4) Vidal, J. L. ; Walker, W. E., Schoening, E. C. $[Rh_{10}P(CO)_{22}]^{3-}$. A Transition-Metal Carbonyl Cluster with a Metal Polyhedron Based on the Bicapped Square Antiprism As Illustrated by the Structural Study of the Benzyltriethylammonium Salt. **1981**, *7*, 238–242.

(5) Vidal, J. L. $[Rh_{10}As(CO)_{22}]^{3-}$. Example of Encapsulation of Arsenic by Transition-Metal Carbonyl Clusters As Illustrated by the Structural Study of the Benzyltriethylammonium Salt. *Inorg. Chem* **1981**, *20*, 243–249.

(6) Chini, Paolo; Martinengo, S.; Ciani, Gianfranco; Sironi Angelo; Longhetti, L.; Heaton, B. T. Synthesis and X-Ray Crystal Structure of the Anion $[Co_6(CO)_{14}(\mu\text{-}CO)_2P]^-$; an Example of a "Semi-Interstitial Phosphide." *J. Chem. Soc., Chem. Comm.* **1979**, 188–189.

(7) Hong, C. S.; Berben, L. A.; Long, J. R. Synthesis and Characterization of a Decacobalt Carbonyl Cluster with Two Semi-Interstitial Phosphorus Atoms. *Dalt. Trans.* **2003**, *505*, 2119–2120.

(8) Dreher, C.; Zabel, M.; Bodensteiner, M.; Scheer, M. $[(CO)_4W(PH_3)_2]$ as Source of Semi-Interstitial Phosphorus Ligands in Cobalt Carbonyl Clusters. *Organometallics* **2010**, *29*, 5187–5191.

(9) Della Pergola, R.; Sironi, A.; Colombo, V.; Garlaschelli, L.; Racioppi, S.; Sironi, A.; Macchi, P. Periodical Trends in $[Co_6E(CO)_{16}]^-$ Clusters: Structural, Synthetic and Energy Changes Produced by Substitution of P with As. *J. Organomet. Chem.* **2017**, *849–850*, 130–136.

(10) Adams, R. D.; Chen, M.; Elpitiya, G.; Potter, M. E.; Raja, R. Iridium−Bismuth Cluster Complexes Yield Bimetallic Nano-Catalysts for the Direct Oxidation of 3-Picoline to Niacin. *ACS Catal.* **2013**, *3*, 3106–3110.

(11) Wang, P.; Song, F.; Amal, R.; Ng, Y. H.; Hu, X. Efficient Water Splitting Catalyzed by Cobalt Phosphide-Based Nanoneedle Arrays Supported on Carbon Cloth. *ChemSusChem* **2016**, *9*, 472–477.

(12) Popczun, E. J.; Read, C. G.; Roske, C. W.; Lewis, N. S.; Schaak, R. E. Highly Active Electrocatalysis of the Hydrogen Evolution Reaction by Cobalt Phosphide Nanoparticles. *Angew. Chemie - Int. Ed.* **2014**, *53*, 5427–5430.

(13) Desai, P.; Ashokaan, N.; Masud, J.; Pariti, A.; Nath, M. Synthesis and Magnetic Properties of Superparamagnetic CoAs Nanostructures. *Mater. Res. Express* **2015**, *2*, 36102.

(14) Macchi, P.; Sironi, A. Chemical Bonding in Transition Metal Carbonyl Clusters: Complementary Analysis of Theoretical and Experimental Electron Densities. *Coordination Chemistry Reviews*. 2003, pp 383–412.

(15) Frenking, G.; Fröhlich, N. The Nature of the Bonding in Transition-Metal Compounds. *Chem. Rev.* **2000**, *100*, 717–774.

(16) Pyykkö, P.; Runeberg, N. Icosahedral WAu_{12}: A Predicted Closed-Shell Species, Stabilized by Aurophilic Attraction and Relativity and in Accord with the 18-Electron Rule. *Angew. Chemie - Int. Ed.* **2002**, *41*, 2174–2176.

(17) Von Hopffgarten, M.; Frenking, G. Building a Bridge between Coordination Compounds and Clusters: Bonding Analysis of the Icosahedral Molecules $[M(ER)_{12}]$ (M = Cr, Mo, W; E = Zn, Cd, Hg). *J. Phys. Chem. A* **2011**, *115*, 12758–12768.

(18) Bader, R. F. W. Atoms in Molecules. *Acc. Chem. Res.* **1995**, *18*, 9–15.

(19) Kitaura, K.; Morokuma, K. A New Energy Decomposition Scheme for Molecular Interactions within the Hartree-Fock Approximation. *Int. J. Quantum Chem.* **1976**, *10*, 325–340.

(20) Blanco, M. A.; Pendás, A. M.; Francisco, E. Interacting Quantum Atoms: A Correlated Energy Decomposition Scheme Based on the Quantum Theory of Atoms in Molecules. *J. Chem. Theory Comput.* **2005**, *1*, 1096–1109.

(21) Wiberg, K. B. Application of the Pople-Santry-Segal CNDO Method to the Cyclopropylcarbinyl and Cyclobutyl Cation and to Bicyclobutane. *Tetrahedron* **1968**, *24*, 1083–1096.

(22) Coppens, P. *X-Ray Charge Densities and Chemical Bonding*; Oxford University Press: New York, 1997.

(23) Farrugia, L. J.; Evans, C. Experimental X-Ray Charge Density Studies on the Binary Carbonyls $Cr(CO)_6$, $Fe(CO)_5$, and $Ni(CO)_4$. *J. Phys. Chem. A* **2005**, *109*, 8834–8848.

(24) Bader, R. F. W.; Macdougall, P. J.; Lau, C. D. H. Bonded and Nonbonded Charge Concentrations and Their Relation to Molecular Geometry and Reactivity. *J. Am. Chem. Soc.* **1984**, *106*, 1594–1605.

(25) Macchi, P. Modern Charge Density Studies: The Entanglement of Experiment and Theory. *Crystallogr. Rev.* **2013**, *19*, 58–101.

(26) Tiana, D.; Francisco, E.; Blanco, M. A.; Macchi, P.; Sironi, A.; Martı, A. Bonding in Classical and Nonclassical Transition Metal Carbonyls: The Interacting Quantum Atoms Perspective. *J. Chem. Theory Comput.* **2009**, 1064–1074.

(27) Cukrowski, I. IQA-Embedded Fragment Attributed Molecular System Energy Change in Exploring Intramolecular Interactions. *Comput. Theor. Chem.* **2015**, *1066*, 62–75.

(28) Badri, Z.; Foroutan-Nejad, C.; Kozelka, J.; Marek, R. On the Non-Classical Contribution in Lone-Pair–π Interaction: IQA Perspective. *Phys. Chem. Chem. Phys.* **2015**, *17*, 26183–26190.

(29) Foroutan-Nejad, C.; Badri, Z.; Marek, R. Multi-Center Covalency: Revisiting the Nature of Anion–π Interactions. *Phys. Chem. Chem. Phys.* **2015**, *17*, 30670–30679.

(30) Bora, P. L.; Novák, M.; Novotný, J.; Foroutan-Nejad, C.; Marek, R. Supramolecular Covalence in Bifurcated Chalcogen Bonding. *Chem. - A Eur. J.* **2017**, *23*, 7315–7323.

(31) Martín Pendás, A.; Blanco, M. A.; Francisco, E. The Nature of the Hydrogen Bond: A Synthesis from the Interacting Quantum Atoms Picture. *J. Chem. Phys.* **2006**, *125*, 184112.

(32) Energy Decomposition Analysis. *WIREs Comput Mol Sci* **2012**, 2: 43–62 doi: 10.1002/wcms.71.

(33) Diefenbach, A.; Bickelhaupt, F. M.; Frenking, G. The Nature of the Transition Metal-Carbonyl Bond and the Question about the Valence Orbitals of Transition Metals. A Bond-Energy Decomposition Analysis of $TM(CO)_6^q$ (TM^q = Hf^{2-}, Ta^-, W, Re^+, Os^{2+}, Ir^{3+}). *J. Am. Chem. Soc.* **2000**, *122*, 6449–6458.

(34) Bickelhaupt, F. M.; Baerends, E. J. Kohn-Sham Density Functional Theory: Predicting and Understanding Chemistry; Wiley-VCH, John Wiley and Sons, I., Ed.; Kenny B. Lipkowitz and

Donald B. Boyd: New York, 2000; Vol. 15, pp 1–86.

(35) SAINT, Version V7.23A, Bruker. SAINT, version V7.23A, Bruker (2003), Bruker AXS Inc., Madison, Wisconsin, USA.

(36) Krause, L.; Herbst-Irmer, R.; Sheldrick, G. M.; Stalke, D. Comparison of Silver and Molybdenum Microfocus X-Ray Sources for Single-Crystal Structure Determination. *J. Appl. Crystallogr.* **2015**, *48*, 3–10.

(37) Macchi, P.; Bürgi, H. B.; Chimpri, A. S.; Hauser, J.; Gál, Z. Low-Energy Contamination of Mo Microsource X-Ray Radiation: Analysis and Solution of the Problem. *J. Appl. Crystallogr.* **2011**, *44*, 763–771.

(38) Agilent Technologies: CrysAlisPRO Software System, Version 1.171.37.35g, Agilent Technologies UK Ltd, Oxford, UK,(2014).; Agilent Technologies: CrysAlisPRO Software system, version 1.171.37.35g, Agilent Technologies UK Ltd, Oxford, UK, (2014).

(39) Sheldrick, G. M. Crystal Structure Refinement with SHELXL. *Acta Crystallogr. Sect. C Struct. Chem.* **2015**, *71*, 3–8.

(40) Sheldrick, G. M. SHELXT - Integrated Space-Group and Crystal-Structure Determination. *Acta Crystallogr. Sect. A Found. Crystallogr.* **2015**, *71*, 3–8.

(41) Volkov, A.; Macchi, P.; Farrugia, L.; Gatti, C.; Mallinson, P.; Richter, T.; Koritsanszky, T. XD2016 - A Computer Program Package for Multipole Refinement, Topological Analysis of Charge Densities and Evaluation of Intermolecular Energies from Experimental and Theoretical Structure Factors, 2016.

(42) Volkov, A.; Macchi, P.; Farrugia, L.; Gatti, C.; Mallinson, P.; Richter, T.; Koritsanszky, T. XD2006 - a Computer Program for Multipole Refinement, Topological Analysis of Charge Densities and Evaluation of Intermolecular Energies from Experimental or Theoretical Structure Factors., 2006.

(43) E.J. Baerends, T. Ziegler, J. Autschbach, D. Bashford, A. Bérces, F.M. Bickelhaupt, C. Bo, P. M.; Boerrigter, L. Cavallo, D.P. Chong, *et al.* ADF2014, SCM, Theoretical Chemistry, Vrije Universiteit, Amsterdam, The Netherlands.

(44) Frisch, M. J.; Trucks, G. W.; Schlegel, H. B.; Scuseria, G. E.; Robb, M. A.; Cheeseman, J. R.; Scalmani, G.; Barone, V.; Mennucci, B.; Petersson, G. A.; *et al.* Gaussian09 Revision B.010. Gaussian, Inc.: Wallingford CT 2010.

(45) Maxwell, P.; Pendás, Á. M.; Popelier, P. L. A. Extension of the Interacting Quantum Atoms (IQA) Approach to B3LYP Level Density Functional Theory (DFT). *Phys. Chem. Chem. Phys.* **2016**, *18*, 20986–21000.

(46) Daudel, R.; Bader, R. F. W.; Stephens, M. E.; Borrett, D. S. The Electron Pair in Chemistry. *Can. J. Chem.* **1974**, *52*, 1310–1320.

(47) Bader, R. F. W.; Stephens, M. E. Spatial Localization of the Electronic Pair and Number Distributions in Molecules. *J. Am. Chem. Soc.* **1975**, *97*, 7391–7399.

(48) Macchi, P.; Garlaschelli, L.; Sironi, A. Electron Density of Semi-Bridging Carbonyls. Metamorphosis of CO Ligands Observed via Experimental and Theoretical Investigations on $[FeCo(CO)_8]^-$. *J. Am. Chem. Soc.* **2002**, *124*, 14173–14184.

(49) Foroutan-Nejad, C.; Shahbazian, S.; Marek, R. Toward a Consistent Interpretation of the QTAIM: Tortuous Link between Chemical Bonds, Interactions, and Bond/line Paths. *Chem. - A Eur. J.* **2014**,

20, 10140–10152.

(50) Macchi, P.; Proserpio, D. M.; Sironi, A. Experimental Electron Density in a Transition Metal Dimer : Metal–Metal and Metal–Ligand Bonds. *J. Am. Chem. Soc.* **1998**, *120*, 13429–13435.

(51) Francisco, E.; Blanco, M. A.; Pendás, A. M. An Electron Number Distribution View of Chemical Bonds in Real Space. *Phys. Chem. Chem. Phys.* **2007**, *9*, 1087–1092.

(52) Tiana, D.; Francisco, E.; Macchi, P.; Sironi, A.; Martín Pendás, A. An Interacting Quantum Atoms Analysis of the Metal–Metal Bond in $[M_2(CO)_8]n$ Systems. *J. Phys. Chem. A* **2015**, *119*, 2153–2160.

(53) Te Velde, G.; Bickelhaupt, F. M.; Baerends, E. J.; Fonseca Guerra, C.; van Gisbergen, S. J. A.; Snijders, J. G.; Ziegler, T. Chemistry with ADF. *J. Comput. Chem.* **2001**, *22*, 931–967.

(54) Chini, P.; Longoni, G.; Albano, V. G. High Nuclearity Metal Carbonyl Clusters. In *Advances in Organometallic Chemistry*; Edited by F.G.A. Stone, R. W., Ed.; 1976; Vol. 14, pp 285–344.

Graphical Table of Content

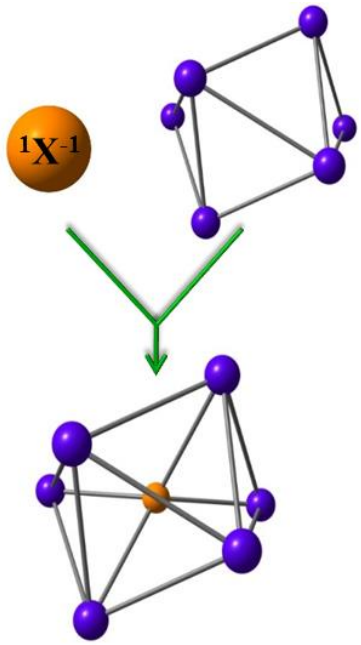

Charge Density and Energy fragment analysis of $[Co_6X(CO)_{16}]^{-1}$ used to analyze the interaction between semi-interstitial atoms and metal-carbonyl cages.